



Systematic Evaluation of DBS Parameters in the Hemi-Parkinsonian Rat Model

Soheil Mottaghi^{1,2,3*}, Oliver Buchholz^{1,2} and Ulrich G. Hofmann^{1,2,3}

¹ Section for Neuroelectronic Systems, Department of Neurosurgery, Medical Center – University of Freiburg, Freiburg, Germany, ² Faculty of Medicine, University of Freiburg, Freiburg, Germany, ³ Technical Faculty, University of Freiburg, Freiburg, Germany

OPEN ACCESS

Edited by:

Hari S. Sharma,
Uppsala University, Sweden

Reviewed by:

Robert Shepherd,
The University of Melbourne, Australia
Seaab Imad Sahib,
University of Arkansas, United States

*Correspondence:

Soheil Mottaghi
soheil.mottaghi@uniklinik-freiburg.de;
soheilmottaghi@gmail.com

Specialty section:

This article was submitted to
Neural Technology,
a section of the journal
Frontiers in Neuroscience

Received: 11 May 2020

Accepted: 03 September 2020

Published: 09 October 2020

Citation:

Mottaghi S, Buchholz O
and Hofmann UG (2020) Systematic
Evaluation of DBS Parameters
in the Hemi-Parkinsonian Rat Model.
Front. Neurosci. 14:561008.
doi: 10.3389/fnins.2020.561008

Electrical stimulation of the subthalamic nucleus (STN) is clinically employed to ameliorate several symptoms of manifest Parkinson's Disease (PD). Stimulation parameters utilized by chronically implanted pulse generators comprise biphasic rectangular short (60–100 μ s) pulses with a repetition frequency between 130 and 180 Hz. A better insight into the effect of electrical stimulation parameters could potentially reveal new possibilities for the improvement of deep brain stimulation (DBS) as a treatment. To this end, we employed single-sided 6-hydroxidopamine (6-OHDA) lesioning of the medial forebrain bundle (MFB) in rats to systematically investigate alternative stimulation parameters. These hemi-parkinsonian (hemi-PD) rats underwent individualized, ipsilateral electrical stimulation to the STN of the lesioned hemisphere, while the transiently induced contralateral rotational behavior was quantified to assess the effect of DBS parameter variations. The number of induced rotations during 30 s of stimulation was strongly correlated with the amplitude of the stimulation pulses. Despite a general linear relation between DBS frequency and rotational characteristics, a plateau effect was observed in the rotation count throughout the clinically used frequency range. Alternative waveforms to the conventional biphasic rectangular (*Rect*) pulse shapes [Triangular (*Tri*), Sinusoidal (*Sine*), and Sawtooth (*Lin.Dec.*)] required higher charges per phase to display similar behavior in rats as compared to the conventional pulse shape. The Euclidean Distance (ED) was used to quantify similarities between different angular trajectories. Overall, our study confirmed that the effect of different amplitude and frequency parameters of STN-DBS in the hemi-PD rat model was similar to those in human PD patients. This shows that induced contralateral rotation is a valuable readout in testing stimulation parameters. Our study supports the call for more pre-clinical studies using this measurement to assess the effect of other DBS parameters such as pulse-width and interphase intervals.

Keywords: systematic DBS evaluation, induced DBS rotation, transient rotation, therapeutic DBS frequency, DBS waveform, DBS amplitude, NES STiM, Unilateral 6-OHDA PD Model

INTRODUCTION

Deep brain stimulation (DBS) has matured over the last decades toward a valuable interventional tool to treat a number of neurological and even psychiatric illnesses: Parkinson's disease (PD) and dystonia have been true ice-breaker applications (Benabid et al., 1991; Tronnier et al., 2002, 2015; Vidailhet et al., 2005; Hardesty and Sackeim, 2007; de Hemptinne et al., 2015), alleviation of chronic pain (Russo and Sheth, 2015) and seizure reduction in epileptics (Velasco et al., 2000; Vonck et al., 2002) were added subsequently. Most recently, obsessive compulsive disorder (OCD) (Alonso et al., 2015), Gilles-de-la-Tourette's syndrome (Almeida et al., 2015) and major depression (Schlaepfer et al., 2013) have been established as targets as well. In all cases, electrical stimulation is applied to a brain region specific to the disease by implanting noble metal electrodes. Electrical parameters are then empirically adjusted to obtain the best treatment outcome. A range of stimulation frequencies (f), amplitudes ($Amp.$), pulse-widths (PW) and pulse shapes have been investigated over the years (Moro et al., 2002; Spieles-Engemann et al., 2010; Gimsa et al., 2011; So et al., 2012; Kang and Lowery, 2014; Khoo et al., 2014; Vallabhajosula et al., 2015; Picillo et al., 2016; Su et al., 2018). However, testing alternative DBS parameters in PD patients can be challenging for ethical, certification and technical reasons, demanding a more versatile platform to study the biological outcomes of DBS parameters.

The unilateral 6-hydroxydopamine (6-OHDA) rat model is one of the more commonly used PD models and has been selected for this study. Unilateral injection of 6-OHDA, a highly specific neurotoxin, into the medial forebrain bundle (MFB) of a rat causes substantial dopamine degeneration at the injection site (ipsilaterally) (Ungerstedt, 1968). The main feature of this model is that it keeps one hemisphere intact while the other hemisphere loses its dopaminergic connections after the 6-OHDA injection. This model is thought to provide sufficient behavioral and electrophysiological similarities to human PD to make it an appropriate platform for pre-clinical PD studies including DBS. A wealth of studies on DBS to the subthalamic nucleus (STN-DBS) have been conducted over the years on the hemi-PD rat model and have proven its versatility (McConnell et al., 2012; So et al., 2012, 2017; Summerson et al., 2014). In this study, we quantified transient contralateral DBS-induced rotations while varying DBS electrical parameters (amplitude, frequency, and particularly waveform). This electrically induced rotation measure was first described by So et al. (2017) and we realized its potential to yield a reliable and quantifiable criterion to further study the electrical parameter space of DBS.

MATERIALS AND METHODS

Female Sprague-Dawley rats (290–330 g; $n = 9$) acquired from Charles River Laboratories were housed for 2 weeks at the animal facility of the University Medical Center in Freiburg prior to any further action. The rats were housed under a 12 h/12 h light-dark cycle and were provided with food and water *ad libitum*. All procedures involving animals were approved by the Animal Care

Committee of the University of Freiburg under proposal G15/031 and performed accordingly.

Electrode Assembly

Bipolar Teflon-coated Platinum/Iridium stimulation electrodes (90% Platinum, 10% Iridium, 50 μm diameter, Science Products GmbH, Germany) were prepared in-house. A 10 cm wire was folded in half and twisted 13 times with a tetrode maker (Tetrode Twister, LabMaker, Germany). Two pins were soldered to the wires and the impedance of the electrodes was checked in a saline solution (0.9% NaCl, Sigma Aldrich GmbH, Germany) in order to ensure the usability of the electrodes prior to implantation. All implanted electrodes had an impedance $<5 \text{ k}\Omega$. The electrodes were disinfected using 70% ethanol and kept in a clean container until the surgery.

Figure 1A shows an example of a bipolar electrode.

Handling and Surgery

Prior to surgery, all rats underwent several days of handling in order to familiarize them with the experimenter and the test apparatus. Rats were anesthetized with oxygen (0.15 l/min) and isoflurane (Abbvie, United States) through an appropriate nose cone; the concentration of anesthetic was initially set to 4% and gradually lowered to 1.5% after placing the animal into the stereotaxic frame (David Kopf, United States). Animal breathing, reflexes and level of anesthesia were monitored throughout the duration of the surgery. Aseptic surgery techniques were applied as described in Richter et al. (2013) and its supplemental video.

Under anesthesia, animals were either lesioned by an injection of 6-OHDA or implanted with the pre-fabricated electrode assemblies at the coordinates shown in the following tables (**Tables 1, 2**). For these procedures, a 0.8 mm \varnothing hole was carefully drilled with a handheld dental drill at the intended implantation site, through which the dura was resected using a fine needle. The micro-injector or electrode assembly, mounted to the frame's micromanipulator, was subsequently lowered manually into position at a rate of approximately 200 $\mu\text{m/s}$, and the skull aperture around the implanted electrode was filled with bone wax. Once in place, the electrode was fixed to a nearby stainless-steel screw anchor (0–80 \times 1/8; Plastics One) using a 2-compound dental cement (Palapress; Heraeus Holding GmbH; Germany). An upward-facing connector, mounted on a custom-made Printed Circuit Board (PCB), was attached to the electrodes and fixed with dental cement. Sprague-Dawley rats received an analgesic immediately before surgery, and for the four subsequent days (Carprieve, 1 ml/kg s.c.; Norbrook, United Kingdom).

Lesioning

6-Hydroxydopamine solution (3.6 mg 6-OHDA in 1.5 ml of 0.2% ascorbic acid solution in 0.9% NaCl, Sigma-Aldrich GmbH, Germany) was freshly prepared prior to each operation, and kept in ice and in the dark throughout each surgery. All the animals ($n = 9$) received lesioning in the MFB of the right hemisphere (see **Table 1**). The 6-OHDA solution was injected using a Hamilton syringe (Hamilton, United States) and a microinjection pump (WPI Instrument, United States) under stereotaxic coordinate control.

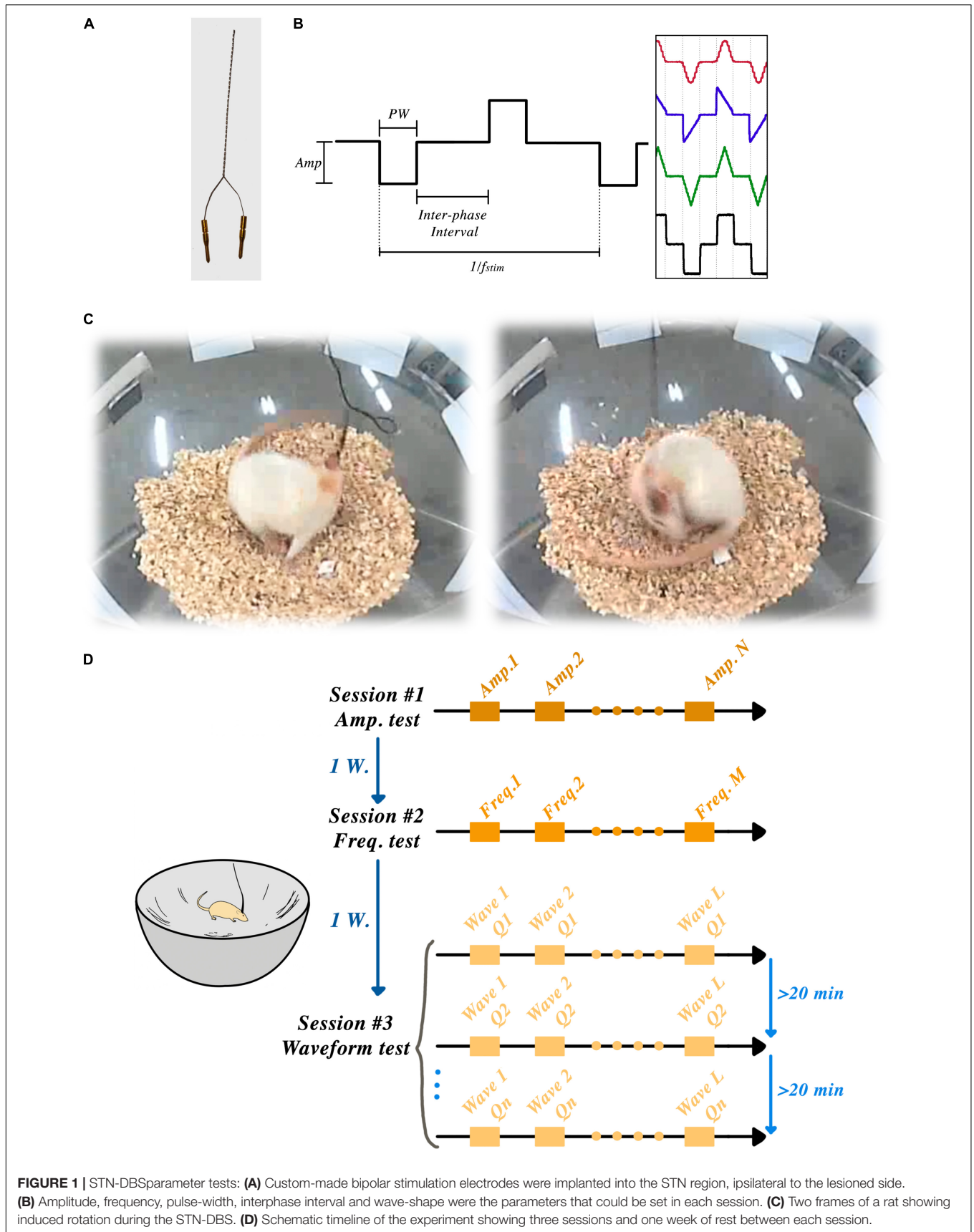


TABLE 1 | Lesioning coordinates in MFB, quantity of 6-OHDA per injection and injection rate.

	AP ¹ (mm)	ML ² (mm)	DV ³ (mm)	Quantity	Injection Speed
MFB	-4.4–4.0	-1.2–0.8	-7.8–7.2	2.5 μl/3.0 μl	1 μl/min/1 μl/min

Coordinates according to (Paxinos et al., 1985). ¹Anterior-Posterior (AP), ²Medial-Lateral (ML), and ³Dorsal-Ventral (DV).

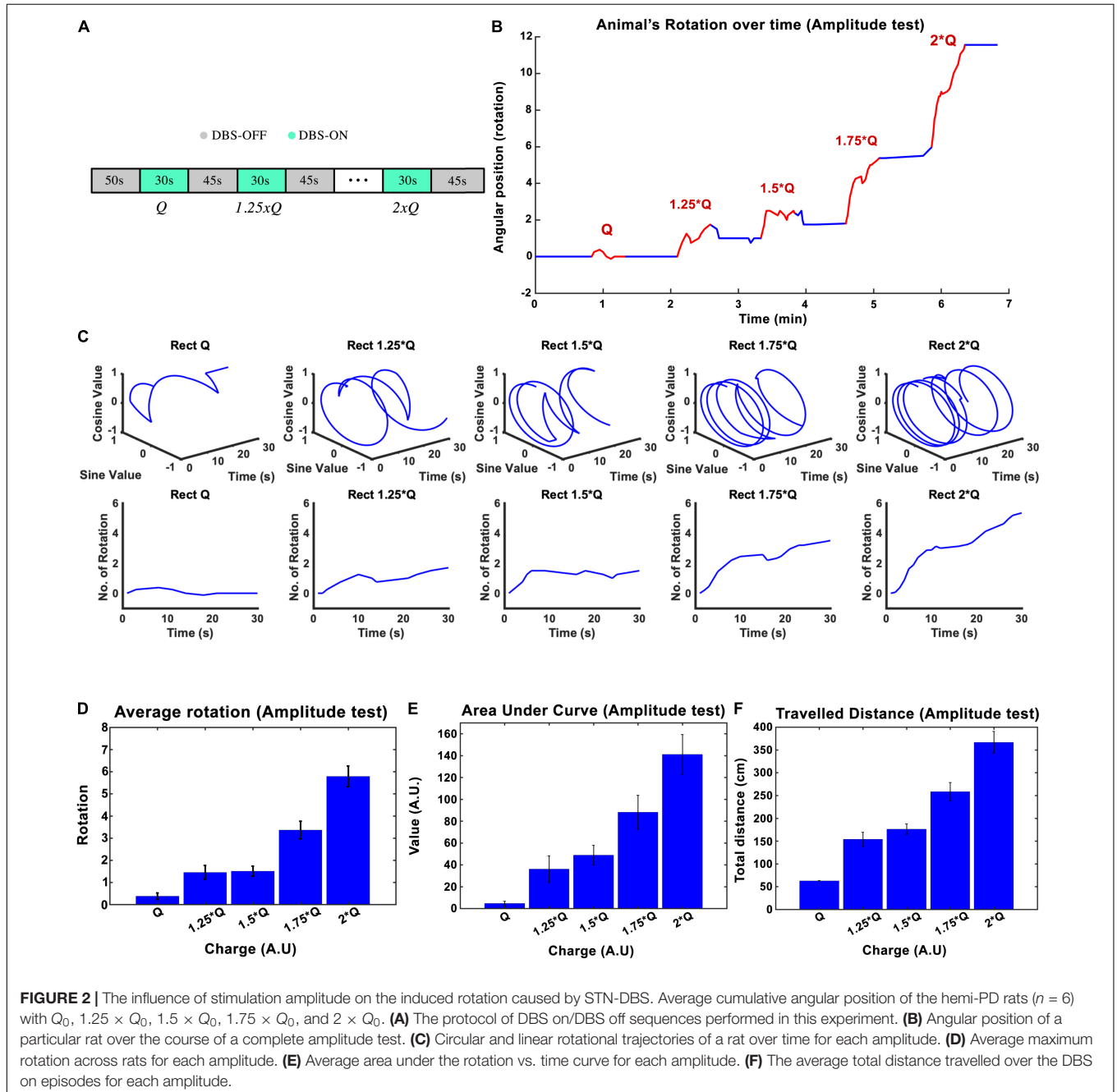
TABLE 2 | Electrode implantation coordinates in M1 and STN.

	AP (mm)	ML (mm)	DV (mm)
M1	+2.5	±3.0	-1.6
STN	-3.8	±2.4	8.0

The canula was left in place for 5 min post-injection, allowing the tissue to absorb the injected volume. The animals received postsurgical care for a week, with diluted

food provided to them and their food and water intake strictly monitored.

The lesion's success was assessed with an apomorphine challenge (Tieu, 2011). Animals showing, on average, at least



three anti-clockwise rotations per minute after a subcutaneous injection of 0.05 mg/kg apomorphine (Sigma Chemicals, Germany; diluted in 0.2% ascorbic acid) for 30 min post-injection were considered well-lesioned.

A week later, all the successfully lesioned rats ($n = 9$) underwent another aseptic surgery to implant bipolar recording electrodes ($\varnothing 50 \mu\text{m}$, 90% Platinum/10% Iridium electrodes, Science Products GmbH, Germany) in the primary motor-cortex (M1) and the STN at the coordinates shown in **Table 2**. All stimulation and recording electrodes were manually assembled under microscope control (see **Figure 1A**) and stereotaxically implanted in

the ipsilateral STN to the lesioned hemisphere (right), as described above.

The reference and ground electrodes were placed above the cerebellum, with the reference electrode implanted sub-durally and the ground electrode connected to a screw fixed in the skull. Similar postsurgical recovery care was provided as that explained in the lesioning section.

Animals were habituated to a corner-free environment (bowl) more than 7 days prior to the experiments. All the electrical stimulation pulses were produced by an open-source, custom-made electrical stimulator: the NES STiM. Detailed system descriptions, as well as a comparison between the NES STiM and

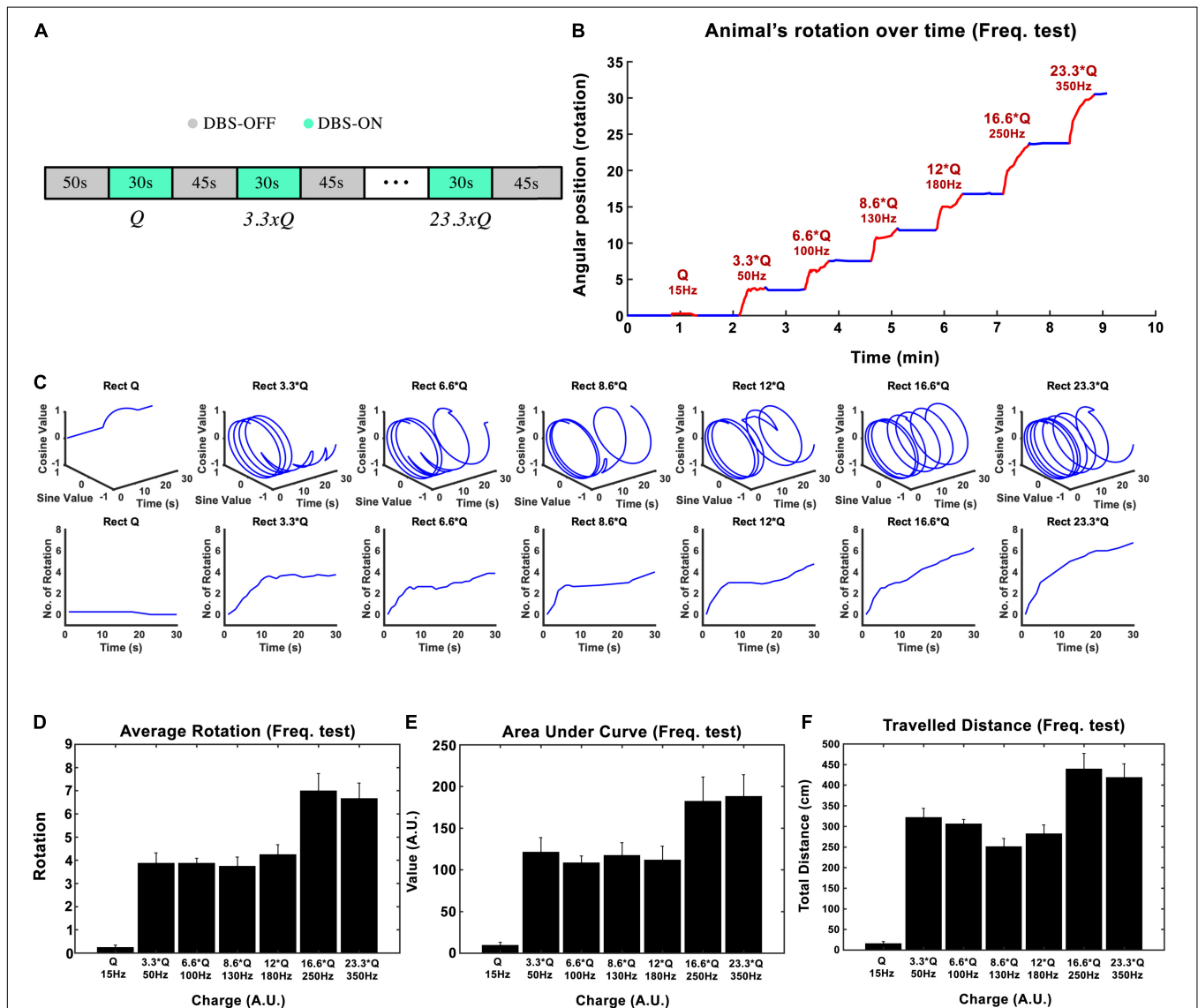


FIGURE 3 | Influence of stimulation frequency on the induced rotation caused by STN-DBS. **(A)** The protocol of DBS on/DBS off sequences performed in this experiment. **(B)** Average accumulative angular position of the hemi-PD rats with 15 Hz (Q_0), 50 Hz ($3.3 \times Q_0$), 100 Hz ($6.6 \times Q_0$), 130 Hz ($8.6 \times Q_0$), 180 Hz ($12 \times Q_0$), 250 Hz ($16.6 \times Q_0$), and 350 Hz ($23.3 \times Q_0$). **(C)** Circular and linear trajectories of the rotations over time for each charge level. **(D)** Average maximum rotation across rats for each frequency. **(E)** Average area under the rotation vs. time curve for each frequency. **(F)** The average total distance travelled over the DBS on episodes for each frequency.

common commercial devices, have been previously published (Mottaghi et al., 2020). In brief, the NES STiM is able to generate four independent biphasic arbitrary current waveforms using four dedicated current source modules. It is designed to be integrated and utilized in pre-clinical and experimental studies, while receiving its stimulation parameters from a computer. The parameters that can be adjusted are shown in **Figure 1B**.

Statistical Analysis

Pearson linear correlation analysis was conducted on the measurements from each experiment to evaluate the strength of association between the variable under study (amplitude, frequency, and charge-waveform) and the rotational results. Additionally, a significance *t*-test was performed on the results

from the waveform experiment to assess the difference between the *Rect* pulses and other waveforms.

Histology

Animals were deeply gas anesthetized immediately after the last experiment. A transcardial perfusion with 4% formaldehyde (PFA in phosphate buffer) was conducted to fix and then extract the brain. The extracted brains were placed in PFA for 7 days and then stored in a 30% sucrose solution. Coronal sections (40 μm) were cut along the implanted electrodes' trajectories (Cryostar NX70, Thermo Fischer scientific, United States) and stored on glass slides at -20°C . Tyrosine hydroxylase (TH) and Nissl staining procedures were performed to assess the dopamine loss and electrode positioning in the brain, respectively.

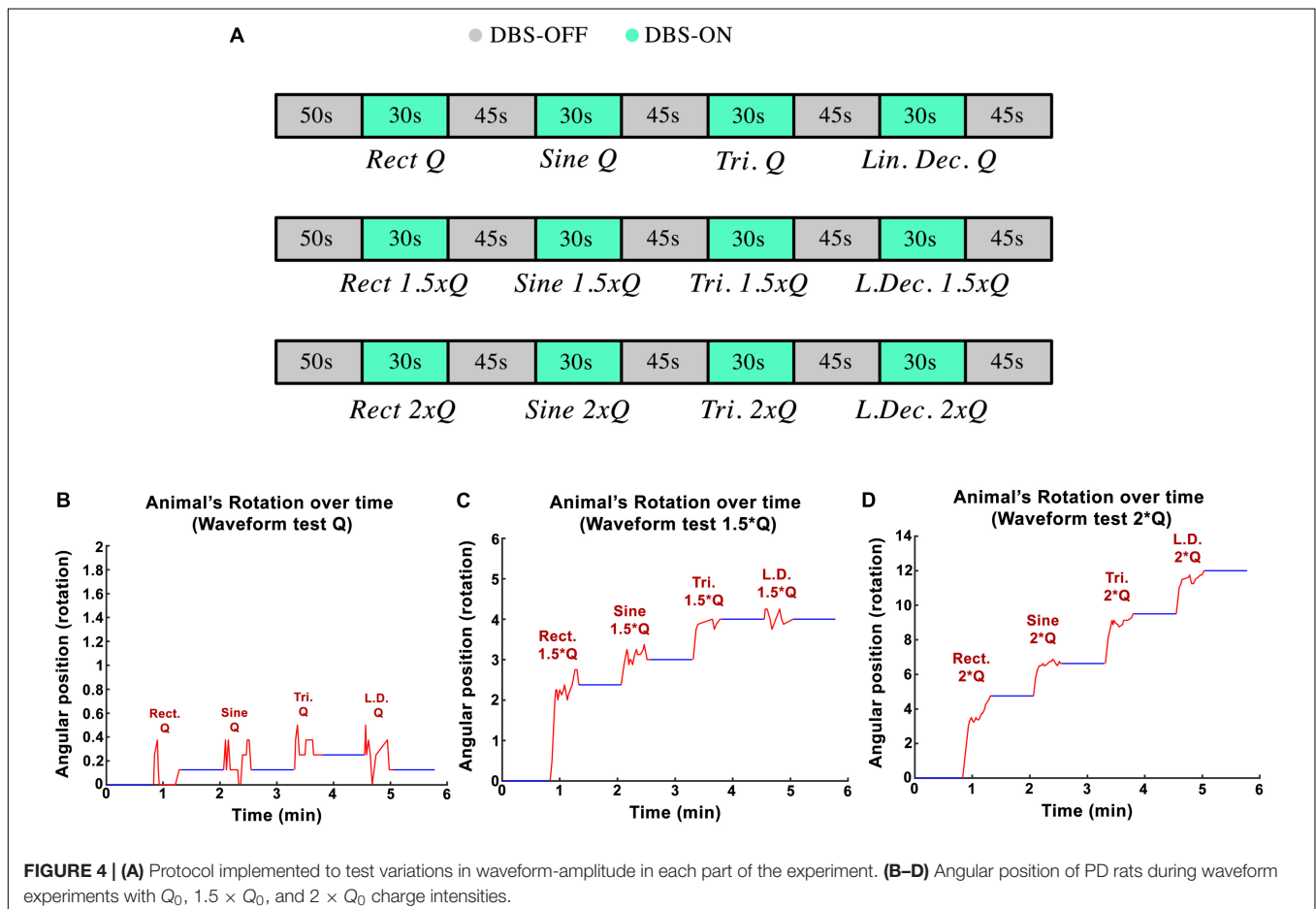
RESULTS

Individualized Current Stimulation Threshold

We used the earlier observation from So et al. (2017) that hemi-PD animals respond to electrical STN stimulation (in absence of any pharmacological stimulus) by rotating along their vertical axis – a behavior demonstrated in **Figure 1C** and usually only

TABLE 3 | Linear correlation analysis results on the three features (total rotation, area under the curve, and the total distance).

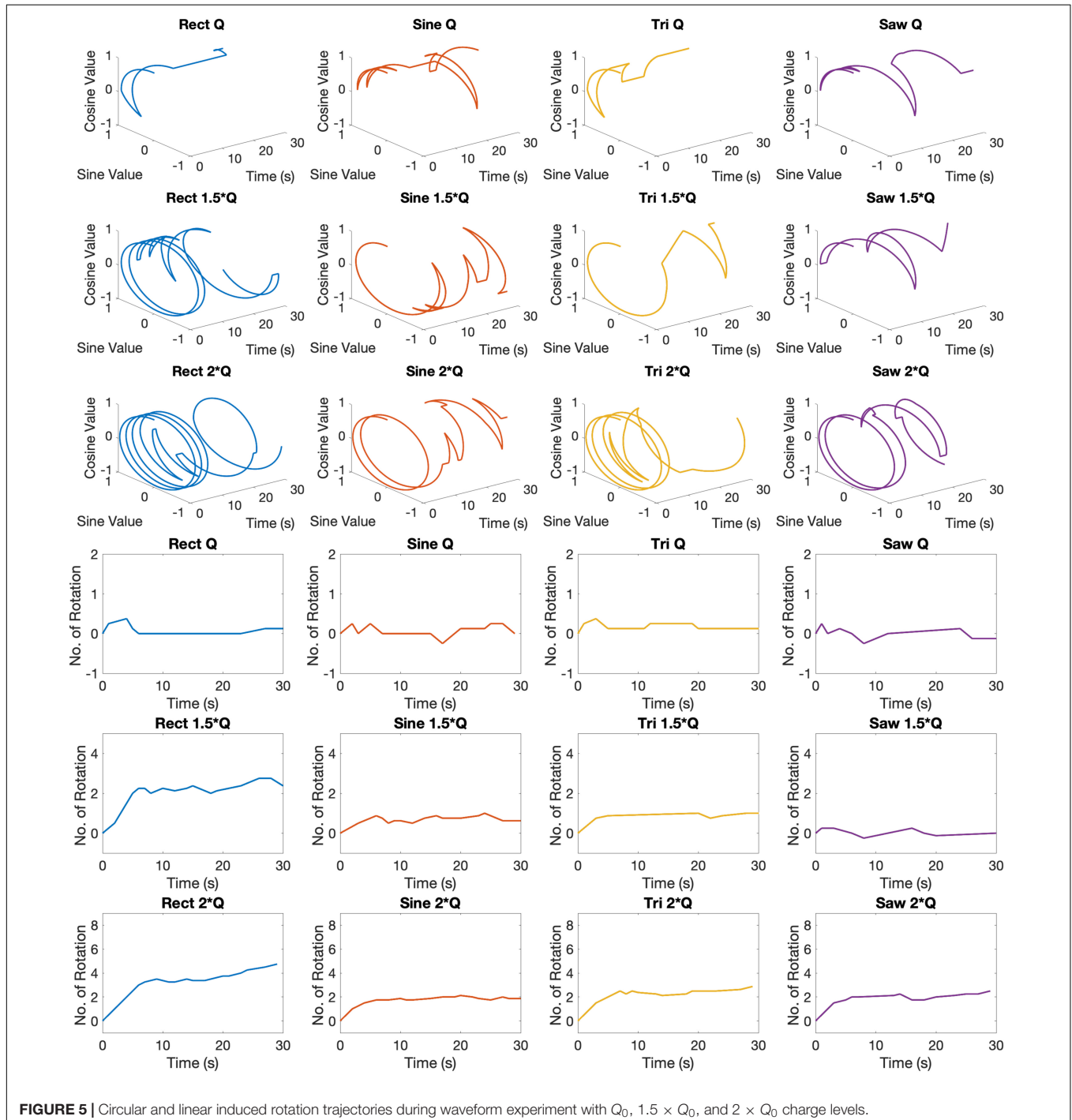
Test		
Total rotation	$\rho_{rot} = 0.894$	$p\text{-Val}_{rot} = 0.007$
Area under the curve	$\rho_{AUC} = 0.863$	$p\text{-Val}_{AUC} = 0.012$
Total distance	$\rho_{TD} = 0.785$	$p\text{-Val}_{TD} = 0.036$



seen after chemical stimuli (e.g., the so-called apomorphine challenge, see above).

After connecting the NES STiM to each animal, a personalized threshold I_0 was found for each rat. I_0 was the smallest current amplitude that induced a transient rotation of less than 180° over 30 s. After this calibration, three rats were excluded from further experiments as they demonstrated an overly sensitive response to stimulation, leading to early dyskinctic side-effects. After finding

the I_0 for each individual animal, they were given a 30-min break before the actual experiments started. The angular position of the rats was measured using a video recording of their behavior throughout the experiment using the BORIS software (Friard and Gamba, 2016) and further analyzed in Matlab (Mathwork, United States). **Figure 1D** illustrates the schematic timeline of the experiments and the corner-free environment that each animal was tested.



Stimulation Paradigm #1: Effects of Variations in Amplitude

The stimulation amplitude was the first parameter that we tested in this study. Biphasic *Rect* pulse trains with a frequency of 130 Hz, 65 μ s PW, and 100 μ s interphase interval were applied (see **Figure 1B** for a representation of the effect of each parameter). During the experiment, an individual rat's stimulation always started with amplitude I_0 and was followed by $1.25 \times I_0$, $1.50 \times I_0$, $1.75 \times I_0$, and $2 \times I_0$, with each stimulation episode lasting for 30 s and leaving a 45-s DBS-off period in between each episode (see **Figure 2A**).

The charge injected in each episode can be calculated as $Q = I \times t$, where I is the current amplitude and t is the duration of the stimulation. The mean \pm standard deviation of the total charge injected from I_0 to $2 \times I_0$ varied from $1.26 \pm 0.38 \mu\text{C/s}$ to $2.53 \pm 0.76 \mu\text{C/s}$ across the six rats that participated in the experiments. A plot of the angular position of one of the hemi-PD animals over the course of the amplitude test is shown in **Figure 2B**, with blue and red lines representing DBS off and on respectively. In order to better visualize the experiment, the individual trajectories of the rat for each 30-s amplitude test episode are pictured using circular plots in **Figure 2C**. I_0 caused, on average, not more than a 1/4 rotation, whereas an amplitude of $2 \times I_0$ induced close to six full rotations during the 30-s episodes (see **Figure 2C**). Pearson's linear correlation coefficient, computed on the total number of rotations per 30-s episode, showed a strong linear relationship between the amplitude and the rotations ($\rho = 0.945$, $p\text{-Val} = 0.015$) (see **Figure 2D**). To include the time-dependent dynamic of the rotations, the area under the time-rotation curve was used as a supplementary measure. It showed an increase from 5 to 141 when the amplitude ramped up from I_0 to $2 \times I_0$, respectively. Clearly, the linear correlation analysis for the area under the curve demonstrated a strong linear relationship with the amplitude as well ($\rho = 0.977$, $p\text{-Val} = 0.004$) (see **Figure 2E**). Under the same testing conditions, the averaged total distance traveled during DBS saw an increase from 62.8 to 366.7 cm with the increase in amplitude, leading to a correlation coefficient of $\rho = 0.982$, and a $p\text{-Val} = 0.003$ (**Figure 2F**).

Stimulation Paradigm #2: Effects of Variations in Frequency

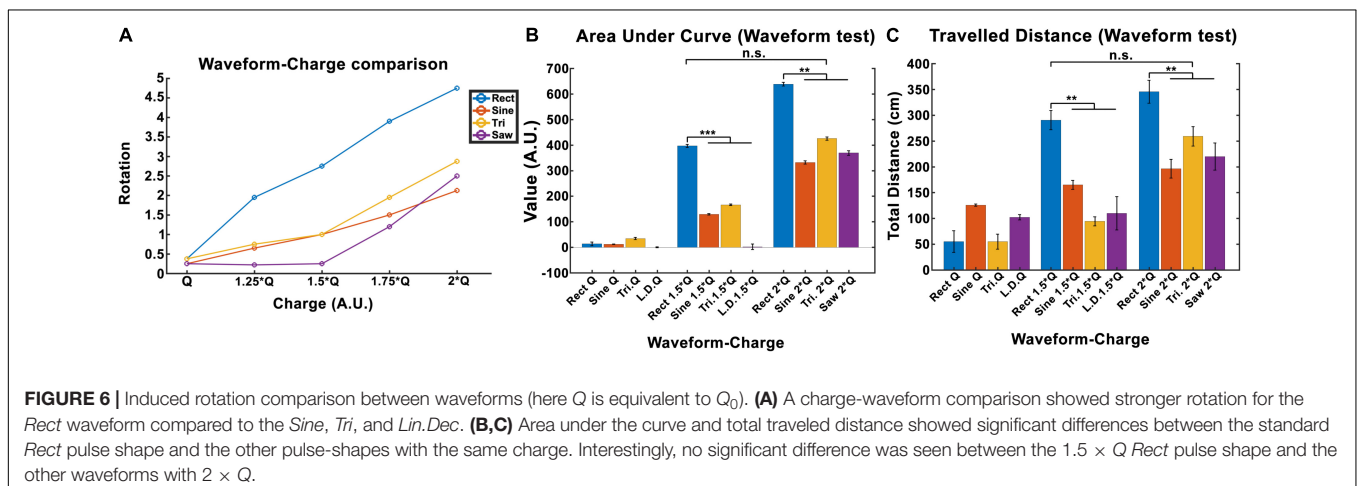
Subthalamic nucleus-deep brain stimulation frequency was tested in the next experimental session. Biphasic *Rect* waveforms with 65 μ s PW and 100 μ s interphase interval were applied. The lowest amplitude at 15 Hz frequency that led to an induced rotation of less than 180-degrees over 30 s was defined to be our I_0 . The current amplitude was left unchanged at this value for the rest of the experiment. Stimulation episodes with 15, 50, 100, 130, 180, 250, and 350 Hz waveforms were applied, each lasting 30 s, with 45-s pauses in between each episode (see **Figure 3A**).

In this experiment, the injected charge per second varied from $0.234 \pm 0.067 \mu\text{C/s}$ at 15 Hz to $5.6 \pm 3.9 \mu\text{C/s}$ at 350 Hz across all the rats ($n = 6$). As an example, the angular position of a particular hemi-PD rat over the course of the experiment is shown in **Figure 3B**. Circular trajectories for each frequency are also depicted in **Figure 3C** to help comprehend the impact of DBS frequency on rotation. The total rotation resulting from DBS rises from 1/4 rotation at 15 Hz to almost four rotations at 50 Hz.

Let's consider the injected charge at 15 Hz as Q_0 . Although the injected charge increases from $3.3 \times Q_0$ at 50 Hz to $12 \times Q_0$ at 180 Hz, the animals' rotations remain almost comparable (see **Figure 3D**). This pattern changes when the number of rotations reaches seven at 250 Hz. Increasing the DBS frequency to 350 Hz did not increase the rotations further. A similar pattern was observed when the area under the curve and total distance were calculated (see **Figures 3E,F**). Linear correlation analysis was performed on all three features (total rotation, area under the curve, and the total distance). The results are presented in **Table 3**.

Stimulation Paradigm #3: Effects of Variations in Waveform-Amplitude

The goal in the third experimental session was to assess the influence of the stimulation pulses' shape on the rotational behavior of the hemi-PD rat model. Standard biphasic *Rect* pulses were compared against *Sine*, symmetric *Tri* and Sawtooth (linear decaying, *Lin. Dec.*) waveforms. The I_0 for the *Rect* waveform was titrated in a



similar manner as in the amplitude paradigm (130 Hz frequency, 100 μ s PW, and 100 μ s interphase interval). The equivalent initial current amplitudes, I_0 , for the different waveforms were calculated in order to keep the charge Q_0 consistent between waveforms. A sequence of *Rect-Sine-Tri-Lin.Dec.* A total of 30-s stimulation episodes with 45-s DBS-off breaks in between was carried out for Q_0 , $1.25 \times Q_0$, $1.5 \times Q_0$, $1.75 \times Q_0$, and $2 \times Q_0$. A 20-min break was given between charges so that the rats could recover (see **Figure 4A**). The animals' average angular position over the course of the stimulation episodes with Q_0 , $1.5 \times Q_0$ and $2 \times Q_0$ are depicted in **Figures 4B–D**.

Examples of circular trajectories for Q_0 , $1.5 \times Q_0$, and $2 \times Q_0$ charge levels are illustrated in **Figure 5**. No alternative waveform (i.e., apart from the biphasic *Rect* pulses) could induce a full rotation with a charge level of Q_0 over the course of a 30-s stimulation episode. An additional 50% increase in charge ($1.5 \times Q_0$) resulted in 2.8 rotations for the *Rect* waveform, while yielding only one full rotation for the *Sine* and *Tri* waveforms and only a quarter rotation for *Lin. Dec.* pulses. The $2 \times Q_0$ charge caused 4.74 rotations on average for *Rect*, 2.12 rotations for *Sine*, 2.87 rotations for *Tri* and 2.49 rotations for *Lin. Dec.* waveforms.

The total locomotion increases with charge for all waveforms, however, the *Rect* waveform produces a distinctly different response compared to the other three waveforms. As presented in **Figure 6A**, *Rect* $1.5 \times Q_0$ and $2 \times Q_0$ resulted in almost twice as many rotations than the other waveforms, which all showed a comparable performance at these charge levels. The average area under the curve and the total traveled distance are depicted for Q_0 , $1.5 \times Q_0$, and $2 \times Q_0$ charge levels in **Figures 6B,C**. Pearson linear correlation coefficients for results from different waveforms are available in **Table 4**.

TABLE 4 | Linear correlation analysis results for different waveforms.

Test		
<i>Rect</i>	rho = 0.993	p-Val = 0.00065
<i>Sine</i>	rho = 0.9931	p-Val = 0.00068
<i>Tri</i>	rho = 0.967	p-Val = 0.007
<i>Lin. Dec.</i>	rho = 0.871	p-Val = 0.054

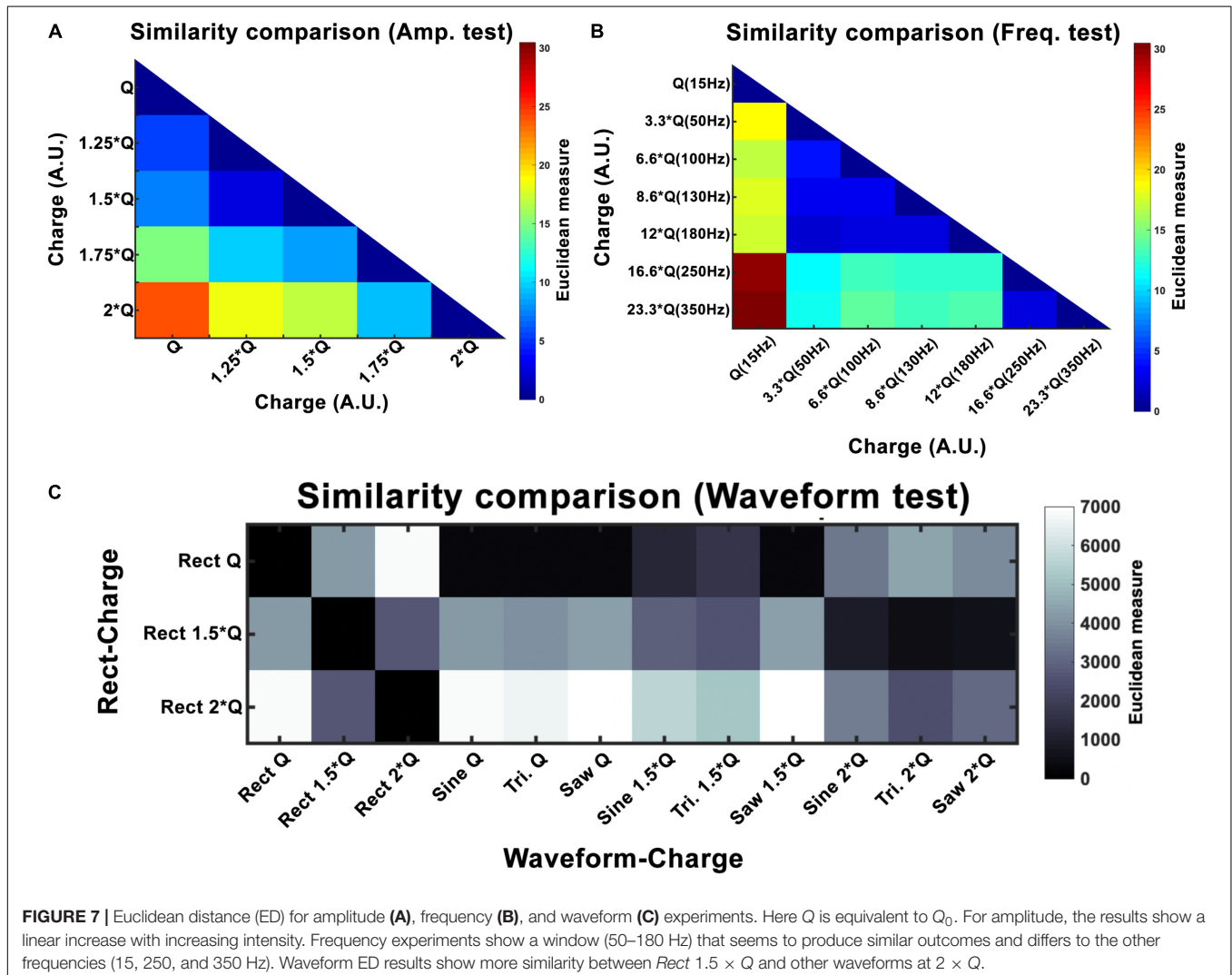


FIGURE 7 | Euclidean distance (ED) for amplitude (A), frequency (B), and waveform (C) experiments. Here Q is equivalent to Q_0 . For amplitude, the results show a linear increase with increasing intensity. Frequency experiments show a window (50–180 Hz) that seems to produce similar outcomes and differs to the other frequencies (15, 250, and 350 Hz). Waveform ED results show more similarity between *Rect* $1.5 \times Q$ and other waveforms at $2 \times Q$.

A significance *t*-test performed on the area under the curve and the total distance features showed that $1.5 \times Q_0$ and $2 \times Q_0$ *Rect* waveform DBS induced significantly more rotations compared to the other waveforms with the same charge. However, no significant difference between the results of $1.5 \times Q_0$ *Rect* and $2 \times Q_0$ of other waveforms was observed (see **Figures 6B,C**).

DISCUSSION

A total of 30-s STN-DBS episodes were systematically applied, assessing a variety of stimulation parameters in hemi-PD rats. A better understanding about the effect of each parameter could potentially disclose great opportunities to improve DBS treatments.

In each experimental paradigm, we tried to alter only one parameter in order to better control the test conditions. Initially, we focused on adjusting the stimulation amplitude. Despite the key role that DBS amplitude plays in DBS calibration procedures, multiple surveys have shown that only fine-tuning the amplitude can lead to side effects such as gait problems, movement interruption and speech impairments (Törnqvist et al., 2005; Moreau et al., 2008; Tommasi et al., 2008; Xie et al., 2012; Tripoliti et al., 2014; Dayal et al., 2017). It has been reported that the total

electrical energy delivered (TEED) has a significant impact on STN-DBS treatments (Schor and Nelson, 2019). TEED can be calculated as follows:

$$TEED = \frac{I^2 \times f \times PW}{Z} \quad (1)$$

where *I* is the current amplitude, *f* stimulation frequency, *PW* pulse-width and *Z* is the electrode-tissue impedance. A study by Schor and Nelson (2019) has reported that the current amplitude has a linear effect on hemi-PD mice’s movement velocities. Our finding also corroborates a strong linear relationship between the amplitude and all the three features we defined (rotation, area under the curve, and total distance). Despite the presented differences between waveforms, this linear relationship remains valid for every waveform we tested. In order to quantify the incrementing similarity across all amplitudes, we computed the Euclidean distance (ED) between the total rotation of all amplitude pairs (see **Figure 7A** and **Table 5**).

Variations in frequency smaller than 50 Hz are repeatedly reported to worsen patients’ symptoms (Moro et al., 2002; Timmermann et al., 2004; Eusebio et al., 2008; Dayal et al., 2017). Frequencies from 50 to 130 Hz are known to cause significant improvements in the symptoms with the best outcomes achieved within the 130–180 Hz range (Moro et al., 2002). It has been shown that the effectiveness of DBS decreases as the frequency surpasses 185 Hz. Clinical studies on stimulation with frequencies above 185 Hz have reported side effects such as lower limb dyskinesias and the sensation of having a heavy head (Moro et al., 2002; Dayal et al., 2017). Studies comparing 60 and 130 Hz stimulations have demonstrated that by maintaining the same total delivered energy, 60 Hz stimulation results in improvements in the occurrence of freezing gait, axial symptoms, akinesia, bradykinesia, and dyskinesias (Moreau et al., 2008; Xie et al., 2012; Khoo et al., 2014; Ramdhani et al., 2015). However, other studies exist which have been unable to show significant differences between 130 Hz and 60–80 Hz stimulation

TABLE 5 | Euclidean distance of rotation trajectories between amplitude pairs under *Rect* stimulation.

	Q_0	$1.25 \times Q_0$	$1.5 \times Q_0$	$1.75 \times Q_0$	$2 \times Q_0$
Q_0	0				
$1.25 \times Q_0$	5.48	0			
$1.5 \times Q_0$	7.38	2.66	0		
$1.75 \times Q_0$	14.85	9.46	8.10	0	
$2 \times Q_0$	23.6	18.20	16.59	9.25	0

TABLE 6 | Euclidean distance (ED) of rotation trajectories between frequency pairs.

	Q_0 (15 Hz)	$3.3 \times Q_0$ (50 Hz)	$6.6 \times Q_0$ (100 Hz)	$8.6 \times Q_0$ (130 Hz)	$12 \times Q_0$ (180 Hz)	$16.6 \times Q_0$ (250 Hz)	$23.3 \times Q_0$ (350 Hz)
Q_0 (15 Hz)	0						
$3.3 \times Q_0$ (50 Hz)	19.04	0					
$6.6 \times Q_0$ (100 Hz)	16.74	4.08	0				
$8.6 \times Q_0$ (130 Hz)	17.94	2.93	2.93	0			
$12 \times Q_0$ (180 Hz)	17.47	2.32	2.66	2.50	0		
$16.6 \times Q_0$ (250 Hz)	29.63	11.43	13.09	12.53	12.72	0	
$23.3 \times Q_0$ (350 Hz)	30.50	11.85	14.10	13.24	13.40	2.60	0

TABLE 7 | Euclidean distance of rotation trajectories between waveform pairs.

	<i>Rect Q</i>	<i>Rect</i> $1.5 \times Q$	<i>Rect</i> $2 \times Q$	<i>Sine Q</i>	<i>Tri Q</i>	<i>Lin.Dec.</i> <i>Q</i>	<i>Sine</i> $1.5 \times Q$	<i>Tri</i> $1.5 \times Q$	<i>Lin. Dec.</i> $1.5 \times Q$	<i>Sine</i> $2 \times Q$	<i>Tri</i> $2 \times Q$	<i>Lin. Dec.</i> $2 \times Q$
<i>RectQ</i>	0	4,216	6,879	252	298	306	1,305	1,666	254	3,435	4,461	3,837
<i>Rect 1.5 × Q</i>	4,216	0	2,715	4,194	3,990	4,339	2,954	2,575	4,338	938	488	577
<i>Rect 2 × Q</i>	6,879	2,715	0	6,859	6,658	7,005	5,630	5,247	7,007	3,535	2,479	3,102

(Brozova et al., 2009; Ricchi et al., 2012; Sidiropoulos et al., 2013; Phibbs et al., 2014). Our results demonstrate similar behavioral effects with a DBS frequency between 50 and 180 Hz. Thus the stimulation's therapeutic frequency window appears to be valid in the 6-OHDA rat model as well. However, rotational behavior was still comparable with a frequency between 250 and 350 Hz, suggesting a ceiling or saturation effect. Our similarity assessments between the frequency pairs show the clear correspondence within the therapeutic frequency windows (see **Figure 7** and **Table 6**).

Reducing the charge per phase in DBS without losing the treatment quality is a desirable goal. Lowering the injected charge would prolong the implantable pulse generator's (IPG) battery life and decrease the probability of tissue damage. Therefore, taking a closer look at the pulse-shape and waveform of the stimulation promises worthwhile for any DBS application. Several studies have attempted to stimulate neural tissue using non-*Rect* waveforms. Among others, *Tri*, *Sine*, gaussian shapes and a few more have been tested and it has been suggested that there might be a more energy efficient waveform than the standard biphasic *Rect* pulses (Sahin and Tie, 2007; Foutz and McIntyre, 2010; Jezernik et al., 2010; Wongsarnpigoon and Grill, 2010).

The computer simulation study done by Sahin and Tie (2007) showed that linearly decreasing ramps (Lin.Dec.) were more efficient than *Rect* pulse shapes. Another study done by Wongsarnpigoon and Grill (2020), involving a computational model of mammalian axons and tested *in vivo* in cat sciatic nerve, showed that a genetic algorithm (GA) optimized waveform could outperform the conventional waveform shapes used for neural tissues. And once again, among the other waveforms, decreasing ramp and decaying exponentials were the most similar waveforms to the GA waveform (difference = ~20%) when PW_{anodic} and $PW_{cathodic}$ were similar and the $PW = 0.05$ ms (Wongsarnpigoon and Grill, 2010).

In our study, normalizing the injected charges to an individualized Q_0 , thus taking biological variations into account, demonstrated only non-significant differences in outcome of alternative waveforms compared to the standard *Rect*. However, when we look at the $1.5 \times Q_0$ and $2 \times Q_0$ charge levels, we see that *Rect* was able to induce more than twice the number of rotations than the other waveforms. In fact, the rotations caused by the $1.5 \times Q_0$ *Rect* waveform were comparable to the rotation results of the other waveforms with $2 \times Q_0$ charge. To quantify and assess this similarity the ED was measured between waveform-amplitude pairs (see **Figure 7C** and **Table 7**). The *Tri* waveform with $2 \times Q_0$, showed the least ED (highest similarity) to the *Rect* $1.5 \times Q_0$ (as highlighted in yellow in **Table 7**).

REFERENCES

- Almeida, L., Martinez-Ramirez, D., Rossi, P. J., Peng, Z., Gunduz, A., and Okun, M. S. (2015). Chasing tics in the human brain: development of open, scheduled and closed loop responsive approaches to deep brain stimulation for tourette syndrome. *J. Clin. Neurol.* 11, 122–131. doi: 10.3988/jcn.2015.11.2.122
- Alonso, P., Cuadras, D., Gabriëls, L., Denys, D., Goodman, W., Greenberg, B. D., et al. (2015). Deep brain stimulation for obsessive-compulsive disorder:

CONCLUSION

Neither PW, nor polarity, wave asymmetry or interphase intervals were varied in this study (Stieger et al., 2020). We thus cannot claim our systematic investigation of different STN-DBS parameters in the hemi-parkinsonian rat to be complete, yet we were already able to show that the transiently induced rotation behavior provides a valuable readout to assess DBS parameters in the hemi-PD rat. Since each single parameter may influence the behavioral result, we suggest to consider all of them with an optimization procedure. During our waveform variation experiments, charges were kept consistent by adjusting the amplitude of the pulses and keeping the PW intact. One can keep the injected charge comparable among the waveforms by using the same amplitude and adjusting the PW.

For future testing, experimental paradigms that randomize the order of each parameter sequence should be considered to avoid possible bias toward stimulation sequences and behavioral outcome. All in all, we suggest the use of the versatile hemi-PD rat model or other similar models to finally sample the full size of DBS's electrical parameter space for the benefit of the patients.

DATA AVAILABILITY STATEMENT

The raw data supporting the conclusions of this article will be made available by the authors, without undue reservation, to any qualified researcher.

ETHICS STATEMENT

The animal study was reviewed and approved by Animal Care Committee of the University of Freiburg under approval G15/031.

AUTHOR CONTRIBUTIONS

SM designed and conducted experimental and analyzed the results. UH supervised the experimental and analysis work. SM, OB, and UH wrote and reviewed the manuscript.

FUNDING

This work is partially supported by the BrainLinks-BrainToolsCluster of Excellence funded by the German Research Foundation (DFG, grant number EXC 1086).

- A meta-analysis of treatment outcome and predictors of response. *PLoS One.* 10:e0133591. doi: 10.1371/journal.pone.0133591
- Benabid, A. L., Pollak, P., Hoffmann, D., Gervason, C., Hommel, M., Perret, J. E., et al. (1991). Long-term suppression of tremor by chronic stimulation of the ventral intermediate thalamic nucleus. *Lancet.* 337, 403–406. doi: 10.1016/0140-6736(91)91175-t
- Brozova, H., Barnaure, I., Alterman, R. L., Tagliati, M., Moreau, C., Destée, A., et al. (2009). STN-DBS frequency effects on freezing of gait in advanced Parkinson disease. *Neurology* 72, 770; author reply 770–771.

- Dayal, V., Limousin, P., and Foltynie, T. (2017). Subthalamic nucleus deep brain stimulation in Parkinson's disease: the effect of varying stimulation parameters. *J. Parkinsons Dis.* 7, 235–245. doi: 10.3233/JPD-171077
- de Hemptinne, C., Swann, N. C., Ostrem, J. L., Ryapolova-Webb, E. S., San Luciano, M., Galifianakis, N. B., et al. (2015). Therapeutic deep brain stimulation reduces cortical phase-amplitude coupling in Parkinson's disease. *Nat. Neurosci.* 18, 779–786. doi: 10.1038/nn.3997
- Eusebio, A., Chen, C. C., Lu, C. S., Lee, S. T., Tsai, C. H., Limousin, P., et al. (2008). Effects of low-frequency stimulation of the subthalamic nucleus on movement in Parkinson's disease. *Exp. Neurol.* 209, 125–130. doi: 10.1016/j.expneurol.2007.09.007
- Foutz, T. J., and McIntyre, C. C. (2010). Evaluation of novel stimulus waveforms for deep brain stimulation. *J. Neural Eng.* 7:066008. doi: 10.1088/1741-2560/7/6/066008
- Friard, O., and Gamba, M. (2016). BORIS: a free, versatile open-source event-logging software for video/audio coding and live observations. *Methods Ecol. Evol.* 7, 1325–1330. doi: 10.1111/2041-210X.12584
- Gimsa, U., Nowak, K., Mix, E., Gimsa, J., Strauss, U., Sriperumbudur, K. K., et al. (2011). Optimizing a rodent model of Parkinson's disease for exploring the effects and mechanisms of deep brain stimulation. *Parkinsons Dis.* 2011:414682. doi: 10.4061/2011/414682
- Hardesty, D. E., and Sackeim, H. A. (2007). Deep brain stimulation in movement and psychiatric disorders. *Biol. Psychiatry.* 61, 831–835. doi: 10.1016/j.biopsych.2006.08.028
- Jezernik, S., Sinkjaer, T., and Morari, M. (2010). Charge and energy minimization in electrical/magnetic stimulation of nervous tissue. *J. Neural Eng.* 7:046004. doi: 10.1088/1741-2560/7/4/046004
- Kang, G., and Lowery, M. M. (2014). Effects of antidromic and orthodromic activation of STN afferent axons during DBS in Parkinson's disease: a simulation study. *Front. Comput. Neurosci.* 8:32. doi: 10.3389/fncom.2014.00032
- Khoo, H. M., Kishima, H., Hosomi, K., Maruo, T., Tani, N., Oshino, S., et al. (2014). Low-frequency subthalamic nucleus stimulation in Parkinson's disease: a randomized clinical trial. *Mov. Disord.* 29, 270–274. doi: 10.1002/mds.25810
- McConnell, G. C., So, R. Q., Hilliard, J. D., Lopomo, P., and Grill, W. M. (2012). Effective deep brain stimulation suppresses low-frequency network oscillations in the basal ganglia by regularizing neural firing patterns. *J. Neurosci.* 32, 15657–15668. doi: 10.1523/JNEUROSCI.2824-12.2012
- Moreau, C., Defebvre, L., Destée, A., Bleuse, S., Clement, F., Blatt, J. L., et al. (2008). STN-DBS frequency effects on freezing of gait in advanced Parkinson disease. *Neurology* 71, 80–84. doi: 10.1212/01.wnl.0000303972.16279.46
- Moro, E., Esselink, R. J. A., Xie, J., Hommel, M., Benabid, A. L., and Pollak, P. (2002). The impact on Parkinson's disease of electrical parameter settings in STN stimulation. *Neurology* 59, 706–713. doi: 10.1212/wnl.59.5.706
- Mottaghi, S., Afshari, N., Buchholz, O., Liebana, S., and Hofmann, U. G. (2020). Modular current stimulation system for pre-clinical studies. *Front. Neurosci.* 14:408. doi: 10.3389/FNINS.2020.00408
- Paxinos, G., Watson, C., Pennisi, M., and Topple, A. (1985). Bregma, lambda and the interaural midpoint in stereotaxic surgery with rats of different sex, strain and weight. *J. Neurosci. Methods* 13, 139–143. doi: 10.1016/0165-0270(85)90026-3
- Phibbs, F. T., Arbogast, P. G., and Davis, T. L. (2014). 60-Hz frequency effect on gait in Parkinson's disease with subthalamic nucleus deep brain stimulation. *Neuromodulation* 17, 717–720. doi: 10.1111/ner.12131
- Picillo, M., Lozano, A. M., Kou, N., Puppi Munhoz, R., and Fasano, A. (2016). Programming deep brain stimulation for Parkinson's disease: the Toronto western hospital algorithms. *Brain Stimul.* 9, 425–437. doi: 10.1016/j.brs.2016.02.004
- Ramdhani, R. A., Patel, A., Swope, D., and Kopell, B. H. (2015). Early use of 60 Hz frequency subthalamic stimulation in Parkinson's disease: a case series and review. *Neuromodulation* 18, 664–669. doi: 10.1111/ner.12288
- Ricchi, V., Zibetti, M., Angrisano, S., Merola, A., Arduino, N., Artusi, C. A., et al. (2012). Transient effects of 80 Hz stimulation on gait in STN DBS treated PD patients: a 15 months follow-up study. *Brain Stimul.* 5, 388–392. doi: 10.1016/j.brs.2011.07.001
- Richter, A., Xie, Y., Schumacher, A., Loeffler, S., Kirch, R., Al-Hasani, J., et al. (2013). A simple implantation method for flexible, multisite microelectrodes into rat brains. *Front. Neuroeng.* 6:6. doi: 10.3389/fneng.2013.00006
- Russo, J. F., and Sheth, S. A. (2015). Deep brain stimulation of the dorsal anterior cingulate cortex for the treatment of chronic neuropathic pain. *Neurosurg. Focus.* 38:E11. doi: 10.3171/2015.3.FOCUS1543
- Sahin, M., and Tie, Y. (2007). Non-rectangular waveforms for neural stimulation with practical electrodes. *J. Neural Eng.* 4, 227–233. doi: 10.1088/1741-2560/4/3/008
- Schlaepfer, T. E., Bewernick, B. H., Kayser, S., Mädler, B., and Coenen, V. A. (2013). Rapid effects of deep brain stimulation for treatment-resistant major depression. *Biol. Psychiatry.* 73, 1204–1212. doi: 10.1016/j.biopsych.2013.01.034
- Schor, J. S., and Nelson, A. B. (2019). Multiple stimulation parameters influence efficacy of deep brain stimulation in Parkinsonian mice. *J. Clin. Investig.* 129, 3833–3838. doi: 10.1172/JCI122390
- Sidiropoulos, C., Walsh, R., Meaney, C., Poon, Y. Y., Fallis, M., and Moro, E. (2013). Low-frequency subthalamic nucleus deep brain stimulation for axial symptoms in advanced Parkinson's disease. *J. Neurol.* 260, 2306–2311. doi: 10.1007/s00415-013-6983-2
- So, R. Q., McConnell, G. C., August, A. T., and Grill, W. M. (2012). Characterizing effects of subthalamic nucleus deep brain stimulation on methamphetamine-induced circling behavior in hemi-Parkinsonian rats. *IEEE Trans. Neural Syst. Rehabil. Eng.* 20, 626–635. doi: 10.1109/TNSRE.2012.2197761
- So, R. Q., McConnell, G. C., and Grill, W. M. (2017). Frequency-dependent, transient effects of subthalamic nucleus deep brain stimulation on methamphetamine-induced circling and neuronal activity in the hemiparkinsonian rat. *Behav. Brain Res.* 320, 119–127. doi: 10.1016/j.bbr.2016.12.003
- Spieles-Engemann, A. L., Collier, T. J., and Sortwell, C. E. (2010). A functionally relevant and long-term model of deep brain stimulation of the rat subthalamic nucleus: advantages and considerations. *Eur. J. Neurosci.* 32, 1092–1099. doi: 10.1111/j.1460-9568.2010.07416.x
- Stieger, K. C., Eles, J. R., Ludwig, K. A., and Kozai, T. D. Y. (2020). In vivo microstimulation with cathodic and anodic asymmetric waveforms modulates spatiotemporal calcium dynamics in cortical neuropil and pyramidal neurons of male mice. *J. Neurosci. Res.* doi: 10.1002/jnr.24676 [Epub ahead of print].
- Su, D., Chen, H., Hu, W., Liu, Y., Wang, Z., Wang, X., et al. (2018). Frequency-dependent effects of subthalamic deep brain stimulation on motor symptoms in Parkinson's disease: a meta-analysis of controlled trials. *Sci. Rep.* 8:14456. doi: 10.1038/s41598-018-32161-3
- Summerson, S. R., Aazhang, B., and Kemere, C. T. (2014). Characterizing motor and cognitive effects associated with deep brain stimulation in the GPI of hemi-Parkinsonian rats. *IEEE Trans. Neural Syst. Rehabil. Eng.* 22, 1218–1227. doi: 10.1109/TNSRE.2014.2330515
- Tieu, K. (2011). A guide to neurotoxic animal models of Parkinson's disease. *Cold Spring Harb. Perspect. Med.* 1:a009316. doi: 10.1101/cshperspect.a009316
- Timmermann, L., Wojtecki, L., Gross, J., Lehrke, R., Voges, J., Maarouf, M., et al. (2004). Ten-hertz stimulation of subthalamic nucleus deteriorates motor symptoms in Parkinson's disease. *Mov. Disord.* 19, 1328–1333. doi: 10.1002/mds.20198
- Tommasi, G., Krack, P., Fraix, V., Le Bas, J. F., Chabardes, S., Benabid, A. L., et al. (2008). Pyramidal tract side effects induced by deep brain stimulation of the subthalamic nucleus. *J. Neurol. Neurosurg. Psychiatry* 79, 813–819. doi: 10.1136/jnnp.2007.117507
- Törnqvist, A. L., Schalén, L., and Rehncrona, S. (2005). Effects of different electrical parameter settings on the intelligibility of speech in patients with Parkinson's disease treated with subthalamic deep brain stimulation. *Mov. Disord.* 20, 416–423. doi: 10.1002/mds.20348
- Tripoliti, E., Limousin, P., Foltynie, T., Candelario, J., Aviles-Olmos, I., Hariz, M. I., et al. (2014). Predictive factors of speech intelligibility following subthalamic nucleus stimulation in consecutive patients with Parkinson's disease. *Mov. Disord.* 29, 532–538. doi: 10.1002/mds.25816
- Tronnier, V. M., Fogel, W., Krause, M., Bonsanto, M. M., Tronnier, J., Heck, A., et al. (2002). High frequency stimulation of the basal ganglia for the treatment of movement disorders: current status and clinical results. *Minim. Invasive Neurosurg.* 45, 91–96. doi: 10.1055/s-2002-32495
- Tronnier, V. M., Domingo, A., Moll, C. K., Rasche, D., Mohr, C., Rosales, R., et al. (2015). Biochemical mechanisms of pallidal deep brain stimulation in X-linked dystonia parkinsonism. *Parkinsonism Relat. Disord.* 21, 954–959. doi: 10.1016/j.parkreldis.2015.06.010

- Ungerstedt, U. (1968). 6-hydroxy-dopamine induced degeneration of central monoamine neurons. *Eur. J. Pharmacol.* 5, 107–110. doi: 10.1016/0014-2999(68)90164-7
- Vallabhajosula, S., Haq, I. U., Hwynn, N., Oyama, G., Okun, M., Tillman, M. D., et al. (2015). Low-frequency versus high-frequency subthalamic nucleus deep brain stimulation on postural control and gait in Parkinson's disease: a quantitative study. *Brain Stimul.* 8, 64–75. doi: 10.1016/j.brs.2014.10.011
- Velasco, A. L., Velasco, M., Velasco, F., Menes, D., Gordon, F., Rocha, L., et al. (2000). Subacute and chronic electrical stimulation of the hippocampus on intractable temporal lobe seizures: preliminary report. *Arch. Med. Res.* 31, 316–328. doi: 10.1016/s0188-4409(00)00064-3
- Vidailhet, M., Vercueil, L., Houeto, J.-L., Krystkowiak, P., Benabid, A.-L., Cornu, P., et al. (2005). Bilateral deep-brain stimulation of the globus pallidus in primary generalized dystonia. *N. Engl. J. Med.* 352, 459–467. doi: 10.1056/NEJMoa042187
- Vonck, K., Boon, P., Achten, E., De Reuck, J., and Caemaert, J. (2002). Long-term amygdalohippocampal stimulation for refractory temporal lobe epilepsy. *Ann Neurol.* 52, 556–565. doi: 10.1002/ana.10323
- Wongsarnpigoon, A., and Grill, W. M. (2010). Energy-efficient waveform shapes for neural stimulation revealed with a genetic algorithm. *J. Neural Eng.* 7:046009. doi: 10.1088/1741-2560/7/4/046009
- Xie, T., Kang, U. J., and Warnke, P. (2012). Effect of stimulation frequency on immediate freezing of gait in newly activated STN DBS in Parkinson's disease. *J. Neurol. Neurosurg. Psychiatry* 83, 1015–1017. doi: 10.1136/jnnp-2011-302091

Conflict of Interest: The authors declare that the research was conducted in the absence of any commercial or financial relationships that could be construed as a potential conflict of interest.

Copyright © 2020 Mottaghi, Buchholz and Hofmann. This is an open-access article distributed under the terms of the Creative Commons Attribution License (CC BY). The use, distribution or reproduction in other forums is permitted, provided the original author(s) and the copyright owner(s) are credited and that the original publication in this journal is cited, in accordance with accepted academic practice. No use, distribution or reproduction is permitted which does not comply with these terms.